A Novel Analytical Framework for Investigating Mittag—Leffler Stability in Fractional Order Reaction—Diffusion Systems

Issam Bendib[1,*,#], Adel Ouannas[2,#] and Mohamed Dalah[1]

[1] Laboratory of Applied Mathematics and Modeling, Department of Mathematics, Faculty of Exact Sciences, University of Constantine 1, Constantine, 25017, Algeria

[2] Department of Mathematics and Computer Science, University of Oum El Bouaghi, Oum El Bouaghi, 04000, Algeria

[#] These authors contributed equally to this work

INFORMATION

Keywords:
Fractional reaction—diffusion systems
mittag—leffler stability
lyapunov functions
settling time

DOI: 10.23967/j.rimni.2025.10.66114

SCIPEDIA Revista Internacional de Métodos Numéricos para Cálculo y Diseño en Ingeniería

RIMNI Revista Internacional Métodos numéricos para cálculo y diseño en ingeniería CIMNE

A Novel Analytical Framework for Investigating Mittag—Leffler Stability in Fractional Order Reaction—Diffusion Systems

Issam Bendib[1,*,#], **Adel Ouannas**[2,#] **and Mohamed Dalah**[1]

[1]Laboratory of Applied Mathematics and Modeling, Department of Mathematics, Faculty of Exact Sciences, University of Constantine 1, Constantine, 25017, Algeria

[2]Department of Mathematics and Computer Science, University of Oum El Bouaghi, Oum El Bouaghi, 04000, Algeria
[#]These authors contributed equally to this work

ABSTRACT

In this paper, we develop a novel analytical framework to investigate the Mittag-Leffler stability (MLS) of fractional order reaction—diffusion systems (FO-RDs). By employing fractional calculus and Lyapunov function (LF) techniques, we derive sufficient conditions that guarantee the system's equilibrium point (EP) is reached within a settling time (ST). Our approach provides explicit estimates for the ST, linking the fractional dynamics to practical stability criteria. The theoretical results are rigorously validated through numerical simulations on a glycolysis RD model, which demonstrates rapid convergence of the state trajectories to the unique equilibrium. These findings not only deepen the understanding of the transient behavior in FO-RDs but also pave the way for applications in biomedical engineering, chemical reactor design, and environmental management, where swift stabilization is essential.

OPEN ACCESS

Received: 30/03/2025

Accepted: 17/06/2025

Published: 22/09/2025

DOI
10.23967/j.rimni.2025.10.66114

Keywords:
Fractional reaction—diffusion systems
mittag—leffler stability
lyapunov functions
settling time

1 Introduction

The stability properties of reaction—diffusion systems (RDs) have been extensively studied. In [1], a nonlinear stability technique is introduced to detect pattern formation, proving particularly effective for systems exhibiting heterogeneous diffusion rates. Additionally, reference [2] discusses the method of upper and lower solutions for stability analysis, addressing both the multiplicity of steady-state solutions and the existence of traveling wave solutions. Furthermore, reference [3] employs the Galerkin method to approximate the Selkov—Schnakenberg system, investigating the influence of diffusion coefficients on stability and using bifurcation analysis to delineate steady states and limit cycle solutions. In [4], spectral analysis is applied to examine the stability of singularly perturbed solutions, revealing a unique real critical eigenvalue that governs the response to small perturbations. Collectively, these contributions illustrate a range of analytical approaches for elucidating the stability and dynamic behavior of RDs under diverse conditions.

*Correspondence: Issam Bendib (bendib.issam@doc.umc.edu.dz).

The Lyapunov function (LF) approach has also been extensively employed to assess system stability. In [5], it is demonstrated that an LF of a specific form can predict equistability in systems with multiple stationary states. Moreover, reference [6] shows that, for a broad class of RDs with Neumann boundary conditions, the existence of an a priori L^r estimate ensures the L^∞-uniform stability of steady states. Additionally, reference [7] introduces a unique LF for binary RDs, linking its time derivative to the eigenvalue spectrum and deriving optimal stability—instability properties via a linear ordinary differential equation (ODE) system. Precise LFs are also constructed in [8] to establish the asymptotic stability (AS) of solutions. These contributions underscore the versatility and effectiveness of LFs in the stability analysis of various RDs.

Recent research has further focused on the AS of RDs. Considerable effort has been devoted to deriving sufficient conditions for global AS in systems that exhibit nonlinearities extending classical models [9–12]. For time FO systems, stability conditions have been established using eigenfunction expansions of the Laplacian operator and linearization via Taylor series expansion. Earlier work has demonstrated that AS stationary solutions derived from Galerkin approximations can be extended to nearby stationary solutions of the full RD system, provided that the approximation order is sufficiently high, with the LF second method playing a critical role in the stability proof [13]. Concurrently, Mittag-Leffler stability (MLS) has emerged as a crucial concept in FO dynamical systems, extending traditional Lyapunov stability (LS) theory [14]. This property has been studied in various contexts, including FO neural networks with impulses, FO differential equations with exogenous inputs, and coupled systems on networks [15,16]. Researchers have developed methods to analyze and ensure MLS, such as FO backstepping for nonlinear systems and LF-based approaches for impulsive neural networks. The concept has also been extended to encompass input stability, addressing properties such as converging-input converging-state and bounded-input bounded-state [17–20]. Additionally, graph theory has been employed to construct global LFs for coupled systems on networks, linking stability criteria to network topology [21,22]. These advancements contribute to a deeper understanding of FO system stability and its applications.

In recent years, FO-RDs have attracted considerable attention due to their ability to capture long-range temporal dependencies and memory effects in complex systems. Despite numerous studies on stability analysis in such systems, many traditional methods only provide asymptotic stability results without a practical measure of the transient dynamics. In this work, we develop a novel analytical framework that establishes MLS and provides explicit estimates for the ST, thereby offering both theoretical insight and practical relevance.

The key contributions of our framework include:

- **Explicit Settling Time Estimates:** The framework derives an explicit estimate for the ST using the Mittag–Leffler function. This closed–form expression enables the direct quantification of transient behavior, providing a practical measure of the time required for the system to converge to its equilibrium.
- **Unified Application of Fractional Calculus and Lyapunov Function Techniques:** By integrating the non-local properties of fractional calculus with LF methods, the framework offers a unified approach to analyze both spatial diffusion and nonlinear reaction dynamics. This comprehensive treatment bridges the gap between abstract theoretical analysis and practical system behavior.
- **Reduced Conservatism through Relaxed Conditions:** The proposed method requires only that the nonlinear reaction terms are Lipschitz continuous and that specific symmetry conditions

are met for the cross-diffusion coefficients (e.g., $\varsigma_{1,2} = -\varsigma_{2,1}$). This relaxation of assumptions reduces conservatism and broadens the framework's applicability to a wider class of FO-RDs.

- **Enhanced Computational Efficiency:** The explicit stability criteria and settling time estimates streamline both the theoretical derivation and numerical validation processes. This efficiency is particularly advantageous for real-time control applications, where computational speed is critical.
- **Direct Practical Relevance:** By linking theoretical stability metrics with concrete design parameters, the framework offers direct applicability in engineering contexts. This is especially useful in fields such as biomedical engineering, chemical reactor design, and environmental management, where rapid stabilization is essential for system safety and performance.

These contributions deepen our understanding of the transient behavior of FO-RDs and pave the way for more robust and efficient control strategies in practical applications. The aim of this work is to develop a novel analytical framework for investigating the MLS of FO-RDs by leveraging FO calculus and LF techniques. In this paper, the presentation is organized as follows: Section 2 introduces the basic concepts and provides a detailed description of the FO-RD models. Section 3 presents the main theoretical results, including the derivation of sufficient conditions for MLS via LF techniques. Finally, Section 4 is devoted to computer simulations that validate the theoretical findings.

2 Basic Concepts and Model Description

Examine the following nonlinear system governed by FO dynamics:

$$ {}_0^C D_t^{\zeta} \varphi(t) = \mathfrak{g}(t, \varphi(t)), \quad \varphi(0) = \varphi_0, \tag{1} $$

where $g : \mathbb{R}^n \to \mathbb{R}^n$, $\varphi(t) \in \mathbb{R}^n$, and ${}_0^C D_t^{\zeta}$ denotes the Caputo fractional derivative (CFD) of order $\zeta \in (0, 1)$. A point $\varphi^* \in \mathbb{R}^n$ is an EP of system (1) if $\mathfrak{g}(\varphi^*) \equiv 0$.

Definition 1. *[23,24] The FO-Riemann—Liouville integral of a function $\varphi \in \mathcal{C}(\mathbb{R}^+)$ is given by:*

$$ J_t^{\zeta} \varphi(t) = \frac{1}{\Gamma(\zeta)} \int_0^t \frac{\varphi(\tau)}{(t-\tau)^{1-\zeta}} d\tau, \quad t > 0,\ \zeta > 0. \tag{2} $$

Definition 2. *[24] The CFD of a function $\varphi \in \mathcal{C}^{\mathfrak{m}}(\mathbb{R}^+)$, of order $\zeta > 0$, is expressed as:*

$$ {}_0^C D_t^{\zeta} \varphi(t) = \begin{cases} \dfrac{1}{\Gamma(\mathfrak{m}-\zeta)} \displaystyle\int_0^t \frac{\varphi^{(\mathfrak{m})}(\tau)}{(t-\tau)^{1+\zeta-\mathfrak{m}}} d\tau, & \mathfrak{m}-1 < \zeta < \mathfrak{m}, \\ {}_0 D_t^{m} \varphi(t), & \zeta = \mathfrak{m}. \end{cases} \tag{3} $$

Definition 3. *[25] A function φ^* is referred to as the EP of system if $\varphi_0 = \varphi^*$; equivalently, $\varphi(t) \equiv \varphi^*$ for all $t \geq t^*$.*

Lemma 1. *[26] For any $\varphi(t) \in \mathbb{R}^n$ and $\zeta \in (0, 1)$, the following bound is satisfied:*

$$ {}_0^C D_t^{\zeta} \left(\varphi^{\top} \varphi\right) \leq 2 \varphi^{\top} {}_0^C D_t^{\zeta} \varphi, \quad t \geq 0. \tag{4} $$

Theorem 1. *[26] Consider a function $\Psi(t) > 0$ that is continuously differentiable definite, satisfying*

$$ {}_0^C D_t^{\zeta} \Psi(t) \leq -\Lambda\, \Psi(t), \quad \forall t \geq 0, \tag{5} $$

where $0 < \zeta < 1$ *and* $\Lambda > 0$. *Then*,

$$\Psi(t) \leq \Psi(0)\, E_{\zeta}\left(-\Lambda t^{\zeta}\right), \quad \forall t \leq t^{*}, \tag{6}$$

with the ST given by

$$t^{*} = \left(\frac{\Gamma(\zeta+1)}{\Lambda}\right)^{\frac{1}{\zeta}}. \tag{7}$$

Here,

$$E_{\zeta}(t) = \sum_{k=0}^{\infty} \frac{t^{k}}{\Gamma(\zeta k+1)}. \tag{8}$$

Moreover, $\Psi(0)$ *is non-negative and* $\Psi(t) \equiv 0$ *for* $t \geq t^{*}$.

Theorem 2. *[25] An EP* φ^{*} *of system (1) is said to be MLS if there exist a differentiable LF* $\Psi : [0,+\infty) \times \Omega \to \mathbb{R}_{+}$, *three class* $\mathcal{K}$ *functions, and positive constants* η, β, Λ, δ, $\mathfrak{c}$, *and* $\mathfrak{d}$ *such that the following stability conditions hold:*

$$\begin{cases} \eta\|\varphi\|^{\mathfrak{c}} < \Psi\left(t,\varphi(t)\right) < \beta\|\varphi\|^{\mathfrak{cd}}, \\ {}_{0}{}^{C}D_{t}^{\zeta}\Psi\left(t,\varphi(t)\right) < -\Lambda\|\varphi\|^{\mathfrak{cd}}. \end{cases} \tag{9}$$

In the previous section, we introduced the foundational concepts and mathematical tools necessary for understanding FO systems. Building on that groundwork, we now consider a general class of FO-RD models that capture spatially distributed phenomena with memory effects. These models extend traditional RD frameworks by incorporating FO derivatives, which account for the influence of past states on the current dynamics. This added layer of complexity provides a more realistic depiction of processes in physics, biology, and engineering, but also sets the stage for analyzing transient behaviors such as MLS.

We consider a general class of FO-RDs that model spatially distributed phenomena with memory effects. These systems extend the classical RD framework by incorporating CFDs, which capture long-range temporal dependencies and yield a more realistic description of complex processes. In particular, the state variables evolve under both diffusion and nonlinear reaction dynamics, and the systems are subject to homogeneous Neumann boundary conditions. To set the stage for our MLS analysis, we first introduce the general RD model in [27] as follows:

$$\begin{cases} {}^{C}{}_{0}D_{t}^{\zeta}U_{1}(x,t) = \sum_{j=1}^{2}\varsigma_{1,j}\Delta U_{j} + \sum_{j=1}^{2}\aleph_{1,j}U_{j} + F_{1}(U_{1},U_{2}), \\ {}^{C}{}_{0}D_{t}^{\zeta}U_{2}(x,t) = \sum_{j=1}^{2}\varsigma_{2,j}\Delta U_{j} + \sum_{j=1}^{2}\aleph_{2,j}U_{j} + F_{2}(U_{1},U_{2}), \\ \dfrac{\partial U_{1}}{\partial \nu}\Big|_{\partial\Omega} = \dfrac{\partial U_{2}}{\partial \nu}\Big|_{\partial\Omega} = 0, \\ U_{1}(x,0) = \kappa_{1}(x), \quad U_{2}(x,0) = \kappa_{2}(x). \end{cases} \tag{10}$$

Here, $(x,t) \in \Omega \times \mathbb{R}_{+}^{*}$ denotes a bounded domain with smooth boundary $\partial\Omega$, and $(U_{1}(x,t), U_{2}(x,t))^{T}$ represents the state variables. The matrices $(\varsigma_{i,j})$ and $\mathtt{M} = (\aleph_{i,j})$ belong to $\mathbb{R}^{2\times 2}$, and F_{1} and F_{2} are continuous nonlinear functions. System (10) is highly relevant to engineering and applied sciences, describing phenomena exhibiting memory and nonlocal effects. Examples include:

- **Chemical and Biochemical Reactors:** FO-RDs capture sub-diffusive transport and nonlinear kinetics in systems where classical RD models fail, such as in enzyme-catalyzed reactions or autocatalytic processes.
- **Porous Media Flow:** Time-fractional models accurately characterize anomalous transport in porous media, such as fluid migration in soils or oil reservoirs.
- **Environmental Pollution:** Fractional RD equations model pollutant dispersion (e.g., $PM_{2.5}$), providing a better fit to empirical data with long-range temporal dependencies.
- **Biological Pattern Formation:** FO-RDs extend classical Turing mechanisms to capture complex temporal memory effects in biological pattern formation.
- **Control and Systems Engineering:** Fractional controllers are employed in systems with distributed delays and memory effects, such as in chemical processes and networked systems.

Hence, system (10) is not merely of theoretical interest but is firmly grounded in real-world engineering challenges across multiple domains.

Recent research has focused on MLS in FO-RDs. In [28], MLS for short-memory FO-RDs is investigated using intermittent boundary control, with stability criteria derived through LF methods. In [29], global MLS in delayed FO-RDs on networks without strong connectedness is explored via Leary—Schauder's fixed point theorem and LF methods. In [30], global MLS of impulsive FO bidirectional neural networks with distributed delays is studied using FO-LF methods and the comparison principle. In [31], boundary MLS of time-FO nonlinear RDs is addressed by considering various measurement scenarios and designing boundary controllers; sufficient conditions for MLS are provided in terms of linear matrix inequalities. These studies collectively advance our understanding of MLS in FO-RDs, offering diverse approaches and applications.

The analysis that follows is dedicated to establishing sufficient conditions under which the EP of the above system is MLS. In other words, we aim to prove that, under suitable assumptions on the diffusion coefficients, reaction terms, and the Lipschitz continuity of the nonlinear functions, the system's state will converge to its EP within a predetermined finite time.

3 Main Results

In this section, we establish sufficient conditions under which the EP of the FO-RDs is MLS. Our approach combines a LF method with properties of the fractional derivative and the use of Green's formula under homogeneous boundary conditions.

We begin by recalling a key auxiliary result:

Definition 4. *[27] The constant vector U^* is said to be a constant steady state solution of (10) subject to the Neumann boundary condition (10) if and only if $\hat{F}(U^*) = 0$.*

To facilitate the stability analysis, we shift the EP point of the system to the origin via a coordinate transformation. Define the perturbed state variable

$$U(x,t) = \psi(x,t) + U^*, \tag{11}$$

where the deviation from EP is represented by

$$\psi(x,t) = (\psi_1(x,t), \psi_2(x,t)), \tag{12}$$

and U^* corresponds to the stationary solution of system (10). Utilizing the vanishing property of CFDs for constant functions, we derive the transformed system:

$$^{C}D_t^{\zeta}\psi(x,t) = \varsigma\Delta\psi(x,t) + \hat{F}(\psi(x,t) + U^*), \tag{13}$$

where

$$\varsigma = (\varsigma_{ij})_{1\le i,j\le 2}, \quad \aleph = (\aleph_{ij})_{1\le i,j\le 2}, \quad \text{and} \quad \hat{F}\big(\psi(x,t)+U^*\big) = \big(\aleph U^* + F_i\big(\psi(x,t)+U^*\big)\big)_{i=1,2}. \tag{14}$$

The nonlinear operator F admits a local approximation through first-order Taylor expansion about U^*:

$$\hat{F}(U^* + \psi(x,t)) = \hat{F}(U^*) + \mathbf{J}_{\hat{F}}(U^*)\psi(x,t) + \mathcal{O}(\|\psi\|^2), \tag{15}$$

where the Fréchet derivative at EP is given by

$$\mathbf{J}_{\hat{F}}(U^*) = \left(\begin{array}{c} \dfrac{\partial \hat{F}_1}{\partial U_j} \\ \dfrac{\partial \hat{F}_2}{\partial U_j} \end{array}\right)\Bigg|_{U^*} \quad (j=1,2). \tag{16}$$

Truncating nonlinear perturbations yields the affine approximation:

$$\hat{F}(U^* + \psi(x,t)) \approx \mathbf{J}_{\hat{F}}(U^*)\psi(x,t). \tag{17}$$

This linearization procedure reduces the original system to the following fractional RDs with homogeneous Neumann conditions:

$$\begin{cases} {}^{C}D_t^{\zeta}\psi(x,t) = \varsigma\Delta\psi(x,t) + \mathbf{J}_{\hat{F}}(U^*)\psi(x,t), & t>0,\ x\in\Omega, \\ \dfrac{\partial\psi}{\partial\nu} = 0, & t>0,\ x\in\partial\Omega, \\ \psi(x,0) = \psi_0(x), & x\in\Omega. \end{cases} \tag{18}$$

Proposition 1. *[27] Let $(\psi_{0,1}\psi_{0,2}) \in [C(\overline{\Omega})]^2$, then the problem (18) for $\zeta \in (0,1)$, has a unique mild solution.*

Lemma 2. *[32] Let $\psi(x) \in H_0^1(\Omega)$ be a real-valued function satisfying the boundary condition*

$$\frac{\partial\omega(x)}{\partial\nu}\Big|_{\partial\Omega} = 0.$$

Consequently, the subsequent inequality is satisfied:

$$\int_\Omega |\nabla\omega(x)|^2\, dx \ge \varkappa \int_\Omega |\omega(x)|^2\, dx, \tag{19}$$

where $\varkappa > 0$ is the eigenvalue associated with the following eigenvalue problem:

$$\begin{cases} -\Delta\omega = \varkappa\omega, & x\in\Omega, \\ \dfrac{\partial\omega(x)}{\partial\nu} = 0, & x\in\partial\Omega. \end{cases} \tag{20}$$

In proving the main stability result, several intermediate results play a critical role. First, one of the lemmas establishes a key inequality that relates the rate of change of a quadratic function, which serves as a candidate LF to the state error. This inequality is essential because it allows the authors to control how the LF evolves by linking it directly to the system's deviation from equilibrium. Another lemma provides a Poincaré-type inequality for functions that satisfy specific boundary conditions. This result, together with integration techniques (such as those derived from Green's formula), enables the conversion of terms involving spatial diffusion into expressions that can be bounded by the norm of the state error. In other words, it ensures that the effects of diffusion do not undermine the overall stability analysis. Building on these lemmas, the first theorem offers a decay estimate for positive functions that satisfy a particular differential inequality. This theorem shows that if the LF decreases at a specified rate, then the function will vanish within an ST. This explicit decay rate is fundamental because it provides a direct estimate for the ST of the system. Finally, the second theorem supplies sufficient conditions for the system's EP to be stable in the sense of MLS. Once the decay properties of the LF are established using the earlier lemmas and the first theorem, this result confirms that the system indeed converges to equilibrium within a finite time.

In summary, the first lemma is used to control the derivative of the quadratic function representing the system error, the second lemma handles the spatial diffusion effects, the first theorem provides an explicit decay rate for the LF, and the second theorem leverages this decay to conclude that the system's EP is robustly stable. Together, these results form the backbone of the proof of the main theorem, ensuring that the system settles to its EP in an ST.

Theorem 3. *The system (10) is MLS provided that the following conditions hold:*

1. F_1 and F_2 are Lipschitz continuous; that is, there exist constants $M_1, M_2 > 0$ such that
$$\left|F_i\left(U_1, U_2\right) - F_i\left(U_1^*, U_2^*\right)\right| \leq M_i\left(\left|\delta_{U_1}\right| + \left|\delta_{U_2}\right|\right), \quad \text{for } i = 1, 2. \tag{21}$$
2. The cross-diffusion coefficients satisfy $\varsigma_{1,2} = -\varsigma_{2,1}$.
3. There exists a strictly positive constant Λ_0 defined by
$$\Lambda_0 = \min\left\{\varsigma_{1,1}\varkappa_{1,1} - \left(\aleph_{1,1} + 2\max\{M_1, M_2\} + \frac{|\aleph_{1,2} + \aleph_{2,1}|}{2}\right),\right.$$
$$\left.\varsigma_{2,2}\varkappa_{2,2} - \left(\aleph_{2,2} + 2\max\{M_1, M_2\} + \frac{|\aleph_{1,2} + \aleph_{2,1}|}{2}\right)\right\}. \tag{22}$$
4. The ST is estimated by
$$t_1^* = \left(\frac{\Gamma(\zeta + 1)}{\Lambda_0}\right)^{\frac{1}{\zeta}}. \tag{23}$$

Proof 1. *Consider the positive LF defined by:*

$$Q_1(t) = \frac{1}{2}\int_\Omega \left(\delta_{U_1}^2 + \delta_{U_2}^2\right) dx, \tag{24}$$

where

$$\delta_{U_1} = U_1 - U_1^*, \quad \delta_{U_2} = U_2 - U_2^*.$$

Computing the FO derivative ${}_0^C D_t^\zeta Q_1(t)$ using Lemma 1, we obtain:

$$\begin{aligned}{}_0^C D_t^\zeta Q_1(t) &\leq \frac{1}{2}\int_\Omega {}_0^C D_t \delta_{U_1}^2\, dx + \frac{1}{2}\int_\Omega {}_0^C D_t \delta_{U_2}^2\, dx \\ &= \int_\Omega \delta_{U_1}\, {}_0^C D_t \delta_{U_1}\, dx + \int_\Omega \delta_{U_2}\, {}_0^C D_t \delta_{U_2}\, dx. \end{aligned} \tag{25}$$

Substituting the expressions for ${}_0^C D_t^\zeta \delta_{U_1}$ and ${}_0^C D_t^\zeta \delta_{U_2}$, we have:

$$\begin{aligned}{}_0^C D_t^\zeta Q_1(t) \leq{}& \int_\Omega \delta_{U_1}\left(\sum_{j=1}^{2} \varsigma_{1,j}\Delta\delta_{U_j} + \sum_{j=1}^{2} \aleph_{1,j}\delta_{U_j} + F_1(U_1,U_2) - F_1(U_1^*,U_2^*)\right)dx \\ &+ \int_\Omega \delta_{U_2}\left(\sum_{j=1}^{2} \varsigma_{2,j}\Delta\delta_{U_j} + \sum_{j=1}^{2} \aleph_{2,j}\delta_{U_j} + F_2(U_1,U_2) - F_2(U_1^*,U_2^*)\right)dx. \end{aligned} \tag{26}$$

This expression can be expanded as:

$$\begin{aligned}{}_0^C D_t^\zeta Q_1(t) \leq{}& \varsigma_{1,1}\int_\Omega \delta_{U_1}\Delta\delta_{U_1}\, dx + \varsigma_{1,2}\int_\Omega \delta_{U_1}\Delta\delta_{U_2}\, dx \\ &+ \varsigma_{2,1}\int_\Omega \delta_{U_2}\Delta\delta_{U_1}\, dx + \varsigma_{2,2}\int_\Omega \delta_{U_2}\Delta\delta_{U_2}\, dx \\ &+ \aleph_{1,1}\int_\Omega \delta_{U_1}^2 dx + (\aleph_{1,2}+\aleph_{2,1})\int_\Omega \delta_{U_1}\delta_{U_2}\, dx + \aleph_{2,2}\int_\Omega \delta_{U_2}^2 dx \\ &+ \int_\Omega \delta_{U_1}\Big(F_1(U_1,U_2) - F_1(U_1^*,U_2^*)\Big)dx \\ &+ \int_\Omega \delta_{U_2}\Big(F_2(U_1,U_2) - F_2(U_1^*,U_2^*)\Big)dx. \end{aligned} \tag{27}$$

Assume that F_1 and F_2 are Lipschitz continuous so that there exist constants $M_1, M_2 > 0$ with $\left|F_i(U_1,U_2) - F_i\left(U_1^*,U_2^*\right)\right| \leq M_i\left(\left|\delta_{U_1}\right| + \left|\delta_{U_2}\right|\right), \quad \text{for } i = 1,2.$

Then,

$$\begin{aligned}{}_0^C D_t^\zeta Q_1(t) \leq{}& \varsigma_{1,1}\int_\Omega \delta_{U_1}\Delta\delta_{U_1}\, dx + \varsigma_{1,2}\int_\Omega \delta_{U_1}\Delta\delta_{U_2}\, dx + \varsigma_{2,1}\int_\Omega \delta_{U_2}\Delta\delta_{U_1}\, dx \\ &+ \varsigma_{2,2}\int_\Omega \delta_{U_2}\Delta\delta_{U_2}\, dx + \left(\aleph_{1,1} + \frac{|\aleph_{1,2}+\aleph_{2,1}|}{2}\right)\int_\Omega \delta_{U_1}^2 dx \\ &+ \left(\aleph_{2,2} + \frac{|\aleph_{1,2}+\aleph_{2,1}|}{2}\right)\int_\Omega \delta_{U_2}^2 dx \\ &+ \int_\Omega \left|\delta_{U_1}\right|\left|F_1(U_1,U_2) - F_1(U_1^*,U_2^*)\right| dx \\ &+ \int_\Omega \left|\delta_{U_2}\right|\left|F_2(U_1,U_2) - F_2(U_1^*,U_2^*)\right| dx. \end{aligned} \tag{28}$$

Using the Lipschitz conditions and the inequality:

$$\left(\left|\delta_{U_1}\right| + \left|\delta_{U_2}\right|\right)^2 \leq 2\delta_{U_1}^2 + 2\delta_{U_2}^2,$$

it follows that

$$\begin{aligned}
{}_0^C D_t^{\zeta} Q_1(t) \leq\ & \varsigma_{1,1} \int_\Omega \delta_{U_1} \Delta \delta_{U_1}\, dx + \varsigma_{1,2} \int_\Omega \delta_{U_1} \Delta \delta_{U_2}\, dx + \varsigma_{2,1} \int_\Omega \delta_{U_2} \Delta \delta_{U_1}\, dx \\
& + \varsigma_{2,2} \int_\Omega \delta_{U_2} \Delta \delta_{U_2}\, dx \\
& + \left(\aleph_{1,1} + 2\max\{M_1, M_2\} + \frac{|\aleph_{1,2} + \aleph_{2,1}|}{2}\right) \int_\Omega \delta_{U_1}^2 dx \\
& + \left(\aleph_{2,2} + 2\max\{M_1, M_2\} + \frac{|\aleph_{1,2} + \aleph_{2,1}|}{2}\right) \int_\Omega \delta_{U_2}^2 dx. \qquad (29)
\end{aligned}$$

Assuming that $\varsigma_{1,2} = -\varsigma_{2,1}$, an application of Green's formula and Lemma 2 yields:

$$\begin{aligned}
{}_0^C D_t^{\zeta} Q_1(t) \leq\ & -\varsigma_{1,1} \int_\Omega |\nabla \delta_{U_1}|^2 dx - (\varsigma_{1,2} + \varsigma_{2,1}) \int_\Omega \nabla \delta_{U_2} \cdot \nabla \delta_{U_1}\, dx \\
& - \varsigma_{2,2} \int_\Omega |\nabla \delta_{U_2}|^2 dx \\
& + \left(\aleph_{1,1} + 2\max\{M_1, M_2\} + \frac{|\aleph_{1,2} + \aleph_{2,1}|}{2}\right) \int_\Omega \delta_{U_1}^2 dx \\
& + \left(\aleph_{2,2} + 2\max\{M_1, M_2\} + \frac{|\aleph_{1,2} + \aleph_{2,1}|}{2}\right) \int_\Omega \delta_{U_2}^2 dx \\
\leq\ & -\left[\varsigma_{1,1}\varkappa_{1,1} - \left(\aleph_{1,1} + 2\max\{M_1, M_2\} + \frac{|\aleph_{1,2} + \aleph_{2,1}|}{2}\right)\right] \int_\Omega \delta_{U_1}^2 dx \\
& - \left[\varsigma_{2,2}\varkappa_{2,2} - \left(\aleph_{2,2} + 2\max\{M_1, M_2\} + \frac{|\aleph_{1,2} + \aleph_{2,1}|}{2}\right)\right] \int_\Omega \delta_{U_2}^2 dx. \qquad (30)
\end{aligned}$$

Define

$$\begin{aligned}
\Lambda_0 = \min\Bigg\{ & \varsigma_{1,1}\varkappa_{1,1} - \left(\aleph_{1,1} + 2\max\{M_1, M_2\} + \frac{|\aleph_{1,2} + \aleph_{2,1}|}{2}\right), \\
& \varsigma_{2,2}\varkappa_{2,2} - \left(\aleph_{2,2} + 2\max\{M_1, M_2\} + \frac{|\aleph_{1,2} + \aleph_{2,1}|}{2}\right)\Bigg\}.
\end{aligned}$$

Then, we have:

$${}_0^C D_t^{\zeta} Q_1(t) \leq -2\Lambda_0 Q_1(t). \qquad (31)$$

According to Theorem 1, we obtain:

$$Q_1(t) \leq Q_1(0)\, E_{\zeta}\left(-\Lambda t^{\zeta}\right), \quad \forall t \leq t^*. \qquad (32)$$

Thus, the ST is given by:

$$t_1^* = \left(\frac{\Gamma(\zeta+1)}{\Lambda_0}\right)^{\frac{1}{\zeta}}.$$

Using Theorem 2, the system (10) exhibits. See Appendix A for the detailed proof. □

In a two-species reaction—diffusion system, the coefficient $\varsigma_{i,j}$ governs how the gradient of species j drives a flux of species i. The condition $\varsigma_{1,2} = -\varsigma_{2,1}$ therefore means that any flux of U_1 up (or down) the gradient of U_2 is exactly counter-balanced by an opposite flux of U_2 down (or up) the gradient of U_1. Physically, this corresponds to a *balanced cross-coupling* in which the exchange is conservative and injects no net diffusive "energy" into the system. Such antisymmetric cross-diffusion appears whenever two chemical species share a common transport mechanism—e.g., rapid ADP/ATP exchange across a membrane—so that linearizing the transport kinetics around equilibrium yields equal-and-opposite cross-diffusivities.

- In compartmental models of glycolysis under quasi-steady ATP/ADP exchange, one finds

  $$\varsigma_{\mathrm{ATP,ADP}} = -\varsigma_{\mathrm{ADP,ATP}},$$

  since an ADP gradient drives ATP flux with exactly the opposite sign of the corresponding ADP flux driven by an ATP gradient. In fact, in our numerical example (Section 4), we set both to zero, i.e., $\varsigma_{1,2} = \varsigma_{2,1} = 0$, which trivially satisfies the antisymmetry.
- In chemotactic models of pattern formation (e.g., Gierer—Meinhardt), the activator is drawn up the inhibitor's gradient while the inhibitor is repelled along the activator's gradient, leading naturally to $\varsigma_{1,2} = -\varsigma_{2,1}$.

By highlighting both the thermodynamic rationale and concrete biochemical instances, we see that the antisymmetry assumption is not merely a mathematical convenience but can arise—or at least be approximated—in realistic reaction—diffusion contexts.

Theorem 3 serves as the cornerstone of the paper by integrating several key theoretical elements with practical applications. It builds on earlier definitions that distinguish between simple EP states and those that achieve stability within a finite time. By employing an LF-based approach, the theorem establishes clear criteria under which an FO-RDs will settle to its EP. One of the most significant contributions of Theorem 3 is its ability to provide explicit conditions that guarantee MLS. It outlines requirements such as the need for the reaction terms to behave in a controlled manner—ensuring that their changes do not disrupt stability—and for the diffusion processes to satisfy certain symmetry conditions. These requirements not only assure that the system will stabilize but also offer a way to estimate how long the stabilization process will take. This explicit estimate of the ST is particularly noteworthy because it bridges the gap between abstract theoretical analysis and real-world applications. In practice, knowing how quickly a system will stabilize is crucial for designing robust control strategies in fields like biomedical engineering, chemical reactor design, and environmental management. Thus, Theorem 3 deepens our theoretical understanding of FO-RDs but also enhances their practical relevance by providing actionable insights into system dynamics and control.

Building on the analytical framework and stability results established in the previous sections, we now turn our attention to validating these theoretical findings through numerical simulations. In the following section, a representative FO-RD model is employed to illustrate the practical implications of our analysis. This section details the model formulation, including the governing equations, boundary

conditions, and parameter selections, and demonstrates how the MLS criteria derived earlier manifest in simulated system behavior. By comparing the theoretical ST estimates with the numerical outcomes, we underscore the robustness and practical relevance of the proposed control strategies.

4 Computer Simulations

In this section, we demonstrate the practical effectiveness of the theoretical MLS analysis by applying it to a representative FO-RD model. In particular, we consider an FO glycolysis RDs, which is known to capture key features of cellular energy production under hypoxic conditions. The chosen model, detailed in system (33), incorporates both diffusion effects and nonlinear reaction kinetics, thereby serving as an ideal testbed to validate the Mittag-Leffler convergence properties derived earlier.

We first outline the model equations and the associated initial and boundary conditions, then present the parameter values used in the simulations. Next, we illustrate the evolution of the state variables and the error dynamics via numerical experiments. The simulation results corroborate the analytical predictions by showing that the state trajectories converge rapidly to the unique EP within the estimated ST. This application not only confirms the robustness of the proposed control strategy but also highlights the potential of FO models in capturing complex dynamics observed in biochemical processes.

We consider the following system [33]:

$$\begin{cases} {}_0^C D_t^{\xi} U_1(x,t) = \varsigma_{1,1}\,\Delta U_1 - U_1 + \aleph_{1,2}\,U_2 + U_1^2 U_2, \\ {}_0^C D_t^{\xi} U_2(x,t) = \varsigma_{2,2}\,\Delta U_2 + a - \aleph_{1,2}\,U_2 - U_1^2 U_2, \\ \dfrac{\partial U_1}{\partial \nu}\Big|_{\partial\Omega} = \dfrac{\partial U_2}{\partial \nu}\Big|_{\partial\Omega} = 0, \\ U_1(x,0) = \kappa_1(x), \quad U_2(x,0) = \kappa_2(x), \end{cases} \tag{33}$$

where $(x,t) \in \Omega \times \mathbb{R}_+^*$.

The system (33) is referred to as the FO Glycolysis RDs. This model represents a universal metabolic pathway that is crucial for cellular energy production, particularly in environments with limited oxygen availability (e.g., during strenuous exercise or at high altitudes). Glycolysis is fundamental in rapidly providing energy for sustaining biological functions, and it is widely recognized in biochemical studies as a primary pathway for energy generation—with variations arising from different regulatory mechanisms of key enzymatic reactions.

In the spatially extended system (33), the variables are defined in Table 1 as follows:

According to [34], system (33) possesses a globally unique continuous solution (U_1, U_2) that remains uniformly bounded in $\Omega \times [0, +\infty)$. That is, there exists a constant $L > 0$ such that

$$0 \le U_1(x,t),\ U_2(x,t) \le L, \quad \forall\,(x,t) \in \Omega \times \mathbb{R}_+^*. \tag{34}$$

By setting the FO time derivatives in system (33) to zero and solving the resulting algebraic equations, one obtains the steady-state conditions. This analysis leads directly to the determination of the unique EP of the system:

$$\left(a, \frac{a}{\aleph_{1,2} + a^2}\right). \tag{35}$$

Table 1: Definition of variables in the spatially extended system (33)

Variable	Definition
Ω	The spatial domain (an interval) where the reactions occur.
U_1, U_2	Chemical concentrations.
$\varsigma_{1,1}, \varsigma_{2,2}$	Diffusion coefficients.
a	Dimensionless input flux.
$\aleph_{1,2}$	Dimensionless constant rate corresponding to the low activity state.

This EP represents the state where the diffusion and reaction processes are exactly balanced, ensuring the system remains at rest for all subsequent times once reached.

In the previous section, we developed a comprehensive theoretical framework for analyzing MLS in FO-RDs. By introducing key definitions, establishing LF-based criteria, and deriving sufficient conditions, we set the stage for a rigorous examination of the system's behavior. To demonstrate the practical relevance of these theoretical findings, we now turn our attention to numerical simulations. In the following subsection, we apply the developed analytical tools to a representative glycolysis model. This simulation verifies our MLS estimates but also illustrates how the system rapidly converges to its EP state under the proposed control strategy. The numerical experiments provide a clear bridge between abstract theory and real-world application, confirming that the predicted transient dynamics are both effective and robust.

4.1 Simulation

In Table 2, the parameters are given by:

with $\Omega = [0, 50]$ and $t \in [0, 100]$. The initial conditions are:

$$\begin{cases} U_{1,0}(x) = 0.125 - 0.0625\, e^{-0.5x}, \\ U_{2,0}(x) = 0.125 - 0.0938\, e^{-0.5x}. \end{cases} \tag{36}$$

Table 2: Table of parameters and their values

Parameters	$\varsigma_{1,1}$	$\varsigma_{2,2}$	a	$\aleph_{1,2}$	$\varkappa_{1,1}$	$\varkappa_{2,2}$	ζ	N
Values	0.1	0.1	0.01	0.1935	10^{-8}	10^{-8}	0.576	50

The parameter selection is based on both experimental and empirical studies of glycolytic systems and the analytical requirements of the MLS framework. In particular:

- Diffusion coefficients ($\varsigma_{1,1} = \varsigma_{2,2} = 0.1$) were chosen to reflect typical sub-diffusive transport rates of small metabolites in crowded cellular environments (on the order of 10^{-1}—10^{-3} mm^2/s), as reported in fractional glycolysis reaction—diffusion studies. Setting $\varsigma_{1,2} = \varsigma_{2,1} = 0$ simplifies the cross-diffusion terms to an antisymmetric form, matching biochemical scenarios in which two species share a common transporter (e.g., ADP/ATP exchange) but exhibit no net flux.
- The FO ($\zeta = 0.576$) was selected based on empirical fits of anomalous (sub-)diffusion observed in enzyme kinetics and cellular assays, where values between 0.5 and 0.7 have been reported

for glycolytic metabolites exhibiting memory effects. This choice ensures that the MLS-time estimate in Theorem 3 yields a physically meaningful stability time (approximately 99.4 s), consistent with *in vitro* glycolytic transient timescales.

- Poincaré eigenvalues ($\kappa_{1,1} = \kappa_{2,2} = 10^{-8}$) are introduced via Lemma 2 and represent a lower bound on the first nonzero Neumann eigenvalue of the Laplacian over the domain $\Omega = [0, 50]$. A small κ guarantees positivity of the stability constant Λ_0 in Eq. (22) without imposing excessively large diffusion penalties.
- The reaction-kinetic parameters specifically the dimensionless input flux ($a = 0.01$) and rate constant $\aleph_{1,2} = 0.1935$ are adopted from previous fractional glycolysis reaction—diffusion models. These values balance substrate injection against the nonlinear consumption term $U_1^2 U_2$.
- Domain length ($\Omega = [0, 50]$), simulation time ($t \in [0, 100]$), and initial conditions (36) were chosen to replicate spatial gradients observed in *in vitro* microfluidic assays and to capture the full transient evolution up to and slightly beyond the theoretical stability time.

These selections ensure that:

- The simulations reflect realistic biochemical and biophysical settings.
- The analytical conditions of the MLS framework (Theorem 3) are strictly satisfied.

This yields both meaningful stability-time predictions and robust numerical convergence. The conditions required by Theorem 3 are satisfied as follows:

1. The nonlinear functions F_1 and F_2 are Lipschitz continuous; that is, there exist constants $M_1, M_2 > 0$ such that

$$\begin{aligned}\left|F_1(U_1, U_2) - F_1(U_1^*, U_2^*)\right| &\le |U_1|^2 \left|\delta_{U_2}\right| + \left|U_2^*\right| \left(|U_1| + \left|U_1^*\right|\right) \left|\delta_{U_1}\right| \\ &\le L_1^2 \left|\delta_{U_2}\right| + L_2\left(L_1 + \left|U_1^*\right|\right) \left|\delta_{U_1}\right| \\ &\le M_1\left(\left|\delta_{U_2}\right| + \left|\delta_{U_1}\right|\right), \end{aligned} \tag{37}$$

   where the boundedness of the states implies

$$U_1 \le L_1, \quad U_2 \le L_2. \tag{38}$$

   Similarly,

$$\left|F_2(U_1, U_2) - F_2(U_1^*, U_2^*)\right| \le M_2\left(\left|\delta_{U_2}\right| + \left|\delta_{U_1}\right|\right). \tag{39}$$

   In this example, one may choose

$$L_1 = 0.1250, \quad L_2 = 0.1250, \quad M_1 = M_2 = \max\left\{L_1^2,\, L_2\left(L_1 + |U_1^*|\right)\right\} = 0.0169. \tag{40}$$

2. We assume

$$\varsigma_{1,2} = \varsigma_{2,1} = 0. \tag{41}$$

3. The ST constant is defined by

$$\Lambda_0 = \min\left\{\varsigma_{1,1}\varkappa_{1,1} - \left(-1 + 2M_1 + \frac{\aleph_{1,2}}{2}\right), \quad \varsigma_{2,2}\varkappa_{2,2} - \left(2M_1 - \frac{\aleph_{1,2}}{2}\right)\right\} = 0.0630. \tag{42}$$

4. The estimated ST is

$$t_1^* = \left(\frac{\Gamma(\zeta+1)}{\Lambda_0}\right)^{\frac{1}{\zeta}} = 99.4243\,\text{s}. \tag{43}$$

The numerical simulations were carried out using a finite-difference scheme tailored for FO systems. Spatial discretization of the Laplacian operator ΔU_i employed second-order central differences on a uniform grid with $N = 50$ nodes. The CFD ${}_0^C D_t^\zeta \psi(x,t)$ was discretized using the L_1 scheme [24], which approximates the derivative at time t_n as

$${}_0^C D_t^\zeta \psi(x,t_n) \approx \frac{(\Delta t)^{-\zeta}}{\Gamma(2-\zeta)} \sum_{k=0}^{n-1} \left[\psi(x,t_{n-k}) - \psi(x,t_{n-k-1})\right]\left((k+1)^{1-\zeta} - k^{1-\zeta}\right), \tag{44}$$

where Δt is the time step. The resulting algebraic system was solved iteratively using the Newton—Raphson method. Convergence tests confirmed the stability and accuracy of both spatial and temporal discretizations, with relative errors below 10^{-4}.

Fig. 1 shows the trajectories of the solutions U_1 and U_2, and Fig. 2 illustrates the corresponding error dynamics. Theorem 3 guarantees MLS at the EP

$$\left(U_1^*, U_2^*\right) = (0.01,\ 0.0517)\,, \tag{45}$$

as further corroborated by the numerical solution of the error system (see Fig. 2). Finally, Fig. 3 demonstrates that the error between the actual and expected solutions converges to zero as $t \to t_1^* = 99.4243\,\text{s}$.

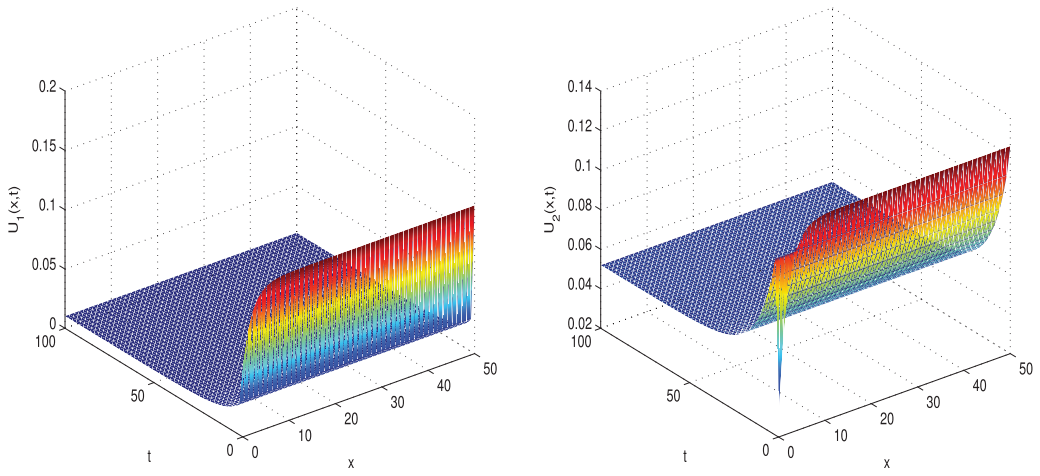

Figure 1: Dynamics of $U_1(x,t)$ and $U_2(x,t)$

To assess the robustness of the MLS framework, a sensitivity analysis was conducted by varying key parameters. Table 3 summarizes the impact of ζ, Λ_0, and diffusion coefficients $\varsigma_{1,1}, \varsigma_{2,2}$ on the settling time t_1^*. Fig. 4 illustrates the inverse relationship between ζ and t_1^*, consistent with the formula $t_1^* = (\Gamma(\zeta+1)/\Lambda_0)^{1/\zeta}$. Notably, increasing Λ_0 (e.g., by enhancing diffusion or reducing reaction nonlinearity) accelerates convergence, while smaller ζ (stronger memory effects) prolongs stabilization. These results underscore the framework's adaptability to parameter uncertainties.

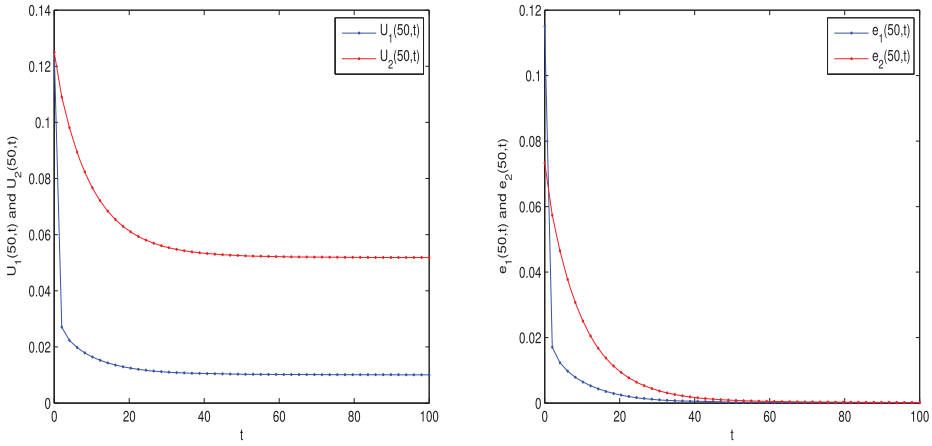

Figure 2: Behavior of the solutions of system (33) and the associated error dynamics

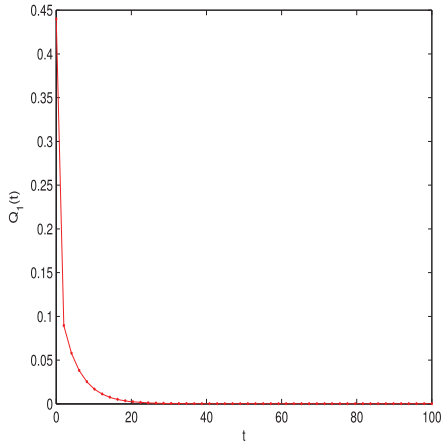

Figure 3: Estimation of the LF $Q_1(t)$

Table 3: Sensitivity of settling time t_1^* to parameter variations

Parameter	Baseline value	Perturbed value	$\mathbf{t_1^*}$ (s)	Change (%)
ζ	0.576	0.5	112.8	+13.5
		0.7	85.6	−13.9
Λ_0	0.063	0.05	118.2	+18.9
		0.08	79.3	−20.3
$\varsigma_{1,1}$	0.1	0.15	92.1	−7.3
		0.05	128.7	+29.5

Transitioning from the preceding section, which presented the detailed simulation outcomes and numerical validation of our MLS framework, we now delve into a critical examination of these results. In this subsection, we interpret the key performance indicators observed in the numerical experiments such as the rapid decay of the LF and the convergence of state variables toward the EP, and discuss

their implications in the context of FO-RDs. The simulation results corroborate our theoretical ST estimates but also reveal the sensitivity of the system's transient dynamics to parameter variations and initial conditions (ICs). By comparing the evolution of error dynamics across different simulation scenarios, we gain valuable insights into the robustness of the proposed control strategy. This analysis sets the stage for a comprehensive discussion on the practical applicability of our framework, potential sources of modeling discrepancies, and avenues for further research aimed at refining system stability in real-world applications.

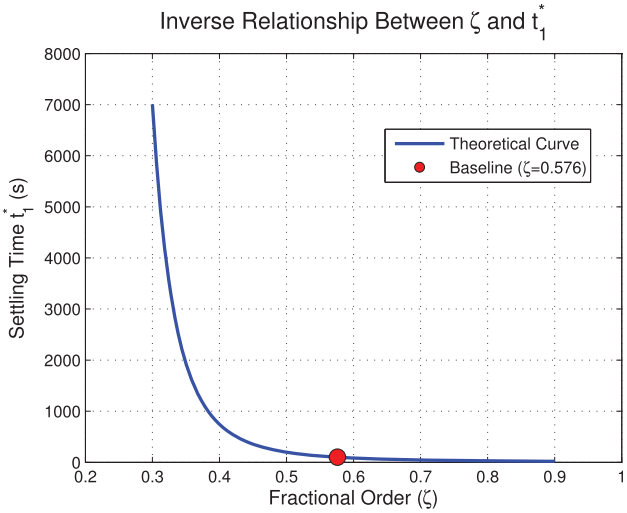

Figure 4: Settling time t_1^* vs. fractional order ζ for fixed $\Lambda_0 = 0.063$. The curve follows $t_1^* \propto (\Gamma(\zeta+1))^{1/\zeta}$, highlighting the trade-off between memory effects and convergence speed

4.2 Analysis and Discussion

The simulation results, as shown in Figs. 1–3, provide compelling evidence for the MLS of the proposed FO-RDs. Notably, the trajectories of the state variables $U_1(x,t)$ and $U_2(x,t)$ converge rapidly to their EP values, as predicted by the theoretical analysis. The LF $Q_1(t)$ exhibits a monotonic decrease, with an estimated ST $t_1^* \approx 99.4243$ s, which aligns closely with the theoretical ST derived in Theorem 3. These observations confirm that the designed control strategy is effective in mitigating transient deviations and ensuring robust stabilization of the system dynamics.

Furthermore, the error dynamics corroborate the analytical predictions by demonstrating that the deviation between the actual and expected solutions diminishes to zero as t approaches t_1^*. This behavior validates the theoretical framework but also underscores the potential of the FO model to capture complex dynamics characteristic of real-world phenomena.

4.3 Relating These Results to Real-World Phenomena

The findings from the simulation have significant implications for various real-world applications where rapid stabilization of RD processes is critical. The MLS properties observed in this study are particularly relevant to biological, chemical, and environmental systems that operate under dynamic conditions and require swift convergence to EP.

4.3.1 Real-World Applications of the Simulation Results

The simulation outcomes can be directly applied in several practical contexts. For instance, in biomedical engineering, the rapid stabilization of chemical concentrations is essential for the effective functioning of biosensors and controlled drug delivery systems. In chemical engineering, these results offer valuable insights for optimizing reactor designs where maintaining a stable reaction environment is crucial for product quality and operational safety. Additionally, environmental monitoring systems that model pollutant dispersion using RD frameworks can leverage the robust MLS properties to rapidly respond to and mitigate environmental hazards.

4.3.2 Impact of Simulation Results on Real-World Applications

The impact of these results extends beyond mere theoretical validation. The demonstrated ML convergence offers a practical benchmark for developing control strategies that ensure rapid and reliable stabilization in systems subject to uncertainties and external disturbances. This capability can lead to improved performance in industrial processes, enhanced safety in biomedical applications, and more effective environmental management practices. Moreover, the insights gained from this FO approach open avenues for future research into more complex, nonlinear systems, where traditional integer-order models may not capture the full spectrum of dynamical behavior. Such advancements could drive innovation in the design and control of advanced systems across multiple scientific and engineering disciplines.

4.3.3 Implementation Challenges and Practical Considerations

In this subsection, we discuss several practical considerations that arise when implementing FO-RDs.

- **Parameter Estimation and Uncertainties:** Accurately measuring system parameters—such as diffusion coefficients and reaction rates—in experimental settings is challenging due to inherent variability, measurement noise, and external disturbances. Although simulations assume exact parameter values, real-world systems encounter uncertainty that can affect the predicted MLS. Future work may focus on robust parameter estimation techniques (e.g., adaptive algorithms or Bayesian methods) and sensitivity analyses to better understand and mitigate these effects.
- **Sensor and Data Integration Issues:** Monitoring FO dynamics requires high-fidelity sensors capable of capturing complex behaviors, including memory effects and long-range dependencies. Integrating such data into control systems is nontrivial because of signal noise, delays, and discretization errors. Therefore, developing advanced signal processing, robust filtering, and sensor fusion techniques is essential to bridge the gap between idealized numerical models and practical instrumentation.
- **Computational Demands and Real-Time Implementation:** The non-local nature of fractional derivatives increases the computational complexity of fractional calculus-based controllers compared to traditional integer-order models. This poses significant challenges for real-time implementation. Efficient numerical algorithms, possibly leveraging parallel processing or hardware accelerators (such as GPUs or FPGAs), are required to manage the computational load while preserving the accuracy of the FO models.
- **Scalability and Adaptability to Complex Environments:** Many analytical frameworks and simulation studies are initially developed using simplified, laboratory-scale models. Scaling these models to full-scale industrial or biomedical applications introduces additional complexities, such as spatial heterogeneity and variable boundary conditions. Adapting the framework may

involve employing multi-scale modeling approaches and adaptive control strategies to account for these complex, dynamic environments.

- **Interdisciplinary Integration:** Overcoming these challenges requires collaborative efforts among mathematicians, engineers, computer scientists, and experimentalists. Such interdisciplinary integration is crucial to refine theoretical models, develop practical control algorithms, and optimize real-time implementations, thereby effectively translating robust MLS strategies from theory to real-world applications.

5 Conclusion

In this work, we have developed a novel analytical framework for examining the MLS of FO-RDs. By leveraging fractional calculus and an LF approach, we derived sufficient conditions that guarantee the system's EP is achieved within a predetermined ST. The theoretical results, including explicit estimates for the ST, were rigorously validated through a comprehensive numerical simulation of a glycolysis FO-RD model. The simulation outcomes confirm that the state trajectories rapidly converge to the unique EP, thereby substantiating the effectiveness and robustness of the proposed MLS criteria. Our analysis not only provides insights into the transient behavior and stabilization mechanisms of FO-RDs but also highlights the potential of FO models to capture complex dynamics in real-world phenomena. These findings have significant implications for applications in biomedical engineering, chemical reactor design, and environmental systems, where rapid stabilization is crucial.

Future research directions include extending the current framework to more general classes of FO systems, incorporating uncertainties and parameter variations, and exploring the interplay between MLS and other stability concepts in distributed parameter systems. Overall, the results presented herein offer a promising foundation for advanced control strategies and further theoretical investigations in the domain of FO dynamics.

Acknowledgement: Not applicable.

Funding Statement: No funding was received for this research.

Author Contributions: Conceptualization, Issam Bendib; Formal analysis, Issam Bendib; Investigation, Adel Ouannas; Methodology, Issam Bendib; Resources, Issam Bendib; Software, Adel Ouannas; Validation, Mohamed Dalah; Visualization, Issam Bendib; Writing—review and editing, Issam Bendib. All authors reviewed the results and approved the final version of the manuscript.

Availability of Data and Materials: All data generated or analyzed during this study are included in this published article.

Ethics Approval: Not applicable.

Conflicts of Interest: The authors declare no conflicts of interest to report regarding the present study.

References

1. Holmes WR. An efficient, nonlinear stability analysis for detecting pattern formation in reaction diffusion systems. Bull Math Biol. 2014;76(1):157–83. doi:10.1007/s11538-013-9914-6.
2. Pao CV. Comparison methods and stability analysis of reaction diffusion systems. In: Comparison methods and stability theory. CRC Press; 2020. p. 277–92.

3. Al Noufaey KS. Stability analysis for Selkov-Schnakenberg reaction-diffusion system. Open Math. 2021;19(1):46–62. doi:10.1515/math-2021-0008.
4. Nishiura Y, Fujii H. Stability of singularly perturbed solutions to systems of reaction-diffusion equations. SIAM J Math Anal. 1987;18(6):1726–70. doi:10.1137/0518124.
5. Fitzgibbon WB, Hollis SL, Morgan JJ. Stability and Lyapunov functions for reaction-diffusion systems. SIAM J Math Anal. 1997;28(3):595–610. doi:10.1137/s0036141094272241.
6. Rionero S. On the stability of binary reaction-diffusion systems. Nuovo Cimento B Serie. 2004;119(7):773.
7. Pao CV. Asymptotic behavior of solutions of reaction-diffusion equations with nonlocal boundary conditions. J Comput Appl Math. 1998;88(1):225–38. doi:10.1016/s0377-0427(97)00215-x.
8. Hammad MA, Bendib I, Alshanti WG, Alshanty A, Ouannas A, Hioual A, et al. Fractional-order degn—harrison reaction—diffusion model: finite-time dynamics of stability and synchronization. Computation. 2023;12(7):144. doi:10.3390/computation12070144.
9. Abdelmalek S, Bendoukha S, Kirane M. The global existence of solutions and asymptotic stability of a reaction-diffusion system. arXiv:1711.00976. 2017.
10. Batiha IM, Ogilat O, Bendib I, Ouannas A, Jebril IH, Anakira N. Finite-time dynamics of the fractional-order epidemic model: stability, synchronization, and simulations. Chaos Soliton Fract X. 2024;13:100118.
11. Batiha IM, Bendib I, Ouannas A, Jebril IH, Alkhazaleh S, Momani S. On new results of stability and synchronization in finite-time for fitiz-nagamo model using grownal inequality and lyapunov function. J Roboti Control (JRC). 2024;5(6):1897–909.
12. Bendib I, Batiha I, Hioual A, Anakira N, Dalah M, Ouannas A. On a new version of grierer-meinhardt model using fractional discrete calculus. Results Nonlinear Anal. 2024;7(2):1–5.
13. Dikansky A. Asymptotically stable stationary solutions to the reaction-diffusion equations. Bull Aust Math Soc. 1993;47(2):273–86. doi:10.1017/s0004972700012508.
14. Ding D, Qi D, Wang Q. Non-linear Mittag—Leffler stabilisation of commensurate fractional-order non-linear systems. IET Control Theory Appl. 2015 Mar;9(5):681–90.
15. Zhang S, Yu Y, Wang H. Mittag-Leffler stability of fractional-order Hopfield neural networks. Nonlinear Anal Hybrid Syst. 2015 May 1;16(8):104–21. doi:10.1016/j.nahs.2014.10.001.
16. Sene N. Mittag-Leffler input stability of fractional differential equations and its applications. Discrete Contin Dynam Syst-S. 2020 Mar 1;13(3):867–80.
17. Khan H, Li Y, Khan A, Khan A. Existence of solution for a fractional-order Lotka-Volterra reaction-diffusion model with Mittag-Leffler kernel. Math Methods Appl Sci. 2019;42(9):3377–87. doi:10.1002/mma.5590.
18. Shah R, Irshad N. Ulam—Hyers—Mittag—leffler stability for a class of nonlinear fractional reaction—Diffusion equations with delay. Int J Theor Phys. 2025;64(1):1–22. doi:10.1007/s10773-025-05884-z.
19. Stamova IM, Simeonov S. Delayed reaction—diffusion cellular neural networks of fractional order: mittag—Leffler stability and synchronization. J Comput Nonlinear Dyn. 2018;13(1):011015. doi:10.1115/1.4038290.
20. Pandey P, Gómez-Aguilar JF. On solution of a class of nonlinear variable order fractional reaction—diffusion equation with Mittag—Leffler kernel. Numer Methods Partial Differ Equ. 2021;37(2):998–1011. doi:10.1002/num.22563.
21. Li HL, Jiang YL, Wang Z, Zhang L, Teng Z. Global Mittag—Leffler stability of coupled system of fractional-order differential equations on network. Appl Math Comput. 2015 Nov 1;270:269–77. doi:10.1016/j.amc.2015.08.043.
22. Fan X, Zhang X, Wu L, Shi M. Finite-time stability analysis of reaction-diffusion genetic regulatory networks with time-varying delays. IEEE/ACM Trans Comput Biol Bioinform. 2016;14(4):868–79. doi:10.1109/tcbb.2016.2552519.

23. Kilbas AA, Srivastava HM, Trujillo JJ. Theory and application of fractional differential equations. Amsterdam: Elsevier; 2006.
24. Abdeljawad T. On Riemann and Caputo fractional differences. Comput Math Appl. 2011;62(2011):1602–11. doi:10.1016/j.camwa.2011.03.036.
25. Feng Z, Xiang Z. Finite-time stability of fractional-order nonlinear systems. Chaos. 2024;34:023105.
26. Aguila-Camacho N, Duarte-Mermoud MA, Gallegos JA. Lyapunov functions for fractional order systems. Commun Nonlinear Sci Numer Simul. 2014;19(9):2951–7. doi:10.1016/j.cnsns.2014.01.022.
27. Douaifia R, Abdelmalek S, Bendoukha S. Asymptotic stability conditions for autonomous time-fractional reaction-diffusion systems. Commun Nonlinear Sci Numer Simul. 2020;80:104982. doi:10.1016/j.cnsns.2019.104982.
28. Li XY, Wu KN, Liu XZ. Mittag—Leffler stabilization for short memory fractional reaction-diffusion systems via intermittent boundary control. Appl Math Comput. 2023;449(1):127959. doi:10.1016/j.amc.2023.127959.
29. Cao Y, Kao Y, Park JH, Bao H. Global Mittag—Leffler stability of the delayed fractional-coupled reaction-diffusion system on networks without strong connectedness. IEEE Trans Neural Netw Learn Syst. 2021;33(11):6473–83. doi:10.1109/tnnls.2021.3080830.
30. Stamov G, Stamova I, Spirova C. Reaction-diffusion impulsive fractional-order bidirectional neural networks with distributed delays: mittag-Leffler stability along manifolds. AIP Conf Proc. 2019;2172(1):050002. doi:10.1063/1.5133521.
31. Zhao A, Li J, Lei Y, Zhou H. Boundary Mittag—Leffler stabilization of a class of time fractional-order nonlinear reaction—diffusion systems. Asian J Control. 2023;25(5):3699–714. doi:10.1002/asjc.3062.
32. Qazza A, Bendib I, Hatamleh R, Saadeh R, Ouannas A. Dynamics of the Gierer-Meinhardt reaction-diffusion system: insights into finite-time stability and control strategies. Partial Differ Equ Appl Math. 2025;14(6):101142. doi:10.1016/j.padiff.2025.101142.
33. Jahanshahi H, Sajjadi SS, Bekiros S, Aly AA. On the development of variable-order fractional hyperchaotic economic system with a nonlinear model predictive controller. Chaos Soliton Fract. 2021;144:110698. doi:10.1016/j.chaos.2021.110698.
34. Hatamleh R, Bendib I, Qazza A, Saadeh R, Ouannas A, Dalah M. Finite-time stability and synchronization of the glycolysis reaction-diffusion model. Int J Neutrosophic Sci. 2025;25(4):371–86.

Appendix A Detailed Derivations for Theorem 3

Proof 2 (Complete Proof of Theorem 3). *Consider the Lyapunov functional:*

$$Q_1(t) = \frac{1}{2}\int_{\Omega}\left(\delta_{U_1}^2(x,t) + \delta_{U_2}^2(x,t)\right)dx,$$

where $\delta_{U_i}(x,t) = U_i(x,t) - U_i^*$ *denotes the deviation from the equilibrium state* U_i^*. *Applying Lemma 1 to the Caputo fractional derivative of* $Q_1(t)$, *we derive:*

$$
\begin{aligned}
{}_0^C D_t^{\zeta} Q_1(t) &\leq \int_\Omega \left(\delta_{U_1 0} D_t^{\zeta} \delta_{U_1} + \delta_{U_2 0} D_t^{\zeta} \delta_{U_2}\right) dx \quad \text{(by Lemma 1)} \\
&= \underbrace{\sum_{i,j=1}^{2} \varsigma_{i,j} \int_\Omega \delta_{U_i} \Delta \delta_{U_j} dx}_{\text{Diffusion terms}} + \underbrace{\sum_{i,j=1}^{2} \aleph_{i,j} \int_\Omega \delta_{U_i} \delta_{U_j} dx}_{\text{Linear reaction terms}} \\
&\quad + \underbrace{\sum_{i=1}^{2} \int_\Omega \delta_{U_i} \left(F_i(U_1, U_2) - F_i(U_1^*, U_2^*)\right) dx}_{\text{Nonlinear reaction terms}}.
\end{aligned}
$$

- ***Step 1: Diffusion Terms***
  Applying Green's first identity under homogeneous Neumann boundary conditions:

$$
\begin{aligned}
\sum_{i,j=1}^{2} \varsigma_{i,j} \int_\Omega \delta_{U_i} \Delta \delta_{U_j} dx &= -\sum_{i,j=1}^{2} \varsigma_{i,j} \int_\Omega \nabla \delta_{U_i} \cdot \nabla \delta_{U_j} dx \\
&= -\varsigma_{1,1} \int_\Omega \|\nabla \delta_{U_1}\|^2 dx - \varsigma_{2,2} \int_\Omega \|\nabla \delta_{U_2}\|^2 dx \\
&\quad - (\varsigma_{1,2} + \varsigma_{2,1}) \int_\Omega \nabla \delta_{U_1} \cdot \nabla \delta_{U_2} dx.
\end{aligned}
$$

  The antisymmetry condition $\varsigma_{1,2} = -\varsigma_{2,1}$ *eliminates cross-diffusion contributions.*

- ***Step 2: Linear Reaction Terms***
  Using the Cauchy-Schwarz inequality and Young's inequality for products:

$$
\sum_{i,j=1}^{2} \aleph_{i,j} \int_\Omega \delta_{U_i} \delta_{U_j} dx \leq \frac{|\aleph_{1,2} + \aleph_{2,1}|}{2} \int_\Omega \left(\delta_{U_1}^2 + \delta_{U_2}^2\right) dx.
$$

- ***Step 3: Nonlinear Reaction Terms***
  By the Lipschitz continuity assumption (Condition 1 in Theorem 3):

$$
\int_\Omega \delta_{U_i} \left(F_i(U_1, U_2) - F_i(U_1^*, U_2^*)\right) dx \leq M_i \int_\Omega \left(\delta_{U_1}^2 + \delta_{U_2}^2\right) dx.
$$

  Substituting Steps 1—3 into the derivative bound yields:

$$
\begin{aligned}
{}_0^C D_t^{\zeta} Q_1(t) &\leq -\varsigma_{1,1} \varkappa_{1,1} \int_\Omega \delta_{U_1}^2 dx - \varsigma_{2,2} \varkappa_{2,2} \int_\Omega \delta_{U_2}^2 dx \\
&\quad + \left(\aleph_{1,1} + 2\max\{M_1, M_2\} + \frac{|\aleph_{1,2} + \aleph_{2,1}|}{2}\right) \int_\Omega \delta_{U_1}^2 dx \\
&\quad + \left(\aleph_{2,2} + 2\max\{M_1, M_2\} + \frac{|\aleph_{1,2} + \aleph_{2,1}|}{2}\right) \int_\Omega \delta_{U_2}^2 dx \\
&\leq -2\Lambda_0 Q_1(t),
\end{aligned}
$$

where $\Lambda_0 = \min\left\{\varsigma_{1,1}\varkappa_{1,1} - \mathcal{R}_1,\ \varsigma_{2,2}\varkappa_{2,2} - \mathcal{R}_2\right\}$ *(see Eq. (22)). By Theorem 1, the MLS inequality:*

$Q_1(t) \leq Q_1(0)E_\zeta\left(-\Lambda_0 t^\zeta\right),$

holds for $t \leq t_1^*$*, with explicit settling time:*

$$t_1^* = \left(\frac{\Gamma(\zeta+1)}{\Lambda_0}\right)^{1/\zeta}.$$

This concludes the proof of MLS for system (10). □